Improved Control Strategy of Current-source Converter for HVDC System

Wenwen Zhang, *Student Member*, *IEEE*, Longlong Chen, Xiaoguang Wei, *Senior Member*, *IEEE*, Lei Qi, Ke Ji, *Member*, *IEEE*, *Member*, *CSEE*, Chong Gao, *Member*, *IEEE*, *Senior Member*, *CSEE*, and Zhiyuan He, *Senior Member*, *IEEE*, *Senior Member*, *CSEE*

***Abstract*—Pulse width modulated current-source converter (PWM-CSC) has great prospects in high voltage direct current transmission system (HVDC) due to its attractive features, such as flexible control characteristics, ability to avoid commutation failure, and lower cost. However, valve voltage of the PWM-CSC is the jump value between filter capacitors line-voltage and zero voltage due to its bypass operation, resulting in high peak voltage withstand by the converter for a rated HVDC system and high voltage ripper ratio. In order to solve these issues, an improved modulation method called specific carrier frequency of SPWM is proposed. After adopting the improved modulation method, the number of the reverse blocking integrated gate commutated thyristor (RB-IGCT) in series can reduce by 31.5% under unity power factor operation and the value of the dc choke can reduce by about 78.6% compared to traditional modulation methods, improving practicability of engineering application. Moreover, active power and reactive power operating range are derived under different modulation methods and the relationship of the power factor, modulation in q-axis and DC current are studied. Finally, effectiveness of the improved modulation method and comparisons of power operating range are verified in PSCAD/EMTDC.**

***Index Terms*—Bypass operation, current source converter (CSC), HVDC system, improved modulation method, operating range of active power and reactive power, valve voltage of the converter.**

I. Introduction

LINE commutated converter technology is playing an important role in high voltage direct current transmission system and asynchronous power grid interconnection because of its attractive features, such as the simplest topology, lowest converter power dissipation, lowest converter cost and mature technology [1]. However, this technology has some unavoidable shortcomings, such as commutation failure, high reactive power consumption, disability to supply passive grid, etc. The modular multilevel converter (MMC) using self-commutated device gives an effective method to overcome these shortcomings in LCC-HVDC system. Also, MMC gives attractive features in renewable energy interconnection such as: active and reactive power decoupled control, the ability to supply passive loads and no commutation failure [2], [3]. Compared to traditional LCC technology, MMC has the disadvantages of high manufacturing cost, small power capacity and high converter loss.

The Hybrid HVDC system consists of LCC applied in rectifier and MMC applied in inverter has the advantages of both: no commutation failure and lower cost, which has been applied in the project [4]–[6]. However, it is more complicated to realize system power reversal, and reducing DC voltage operation due to different characteristics of the converters used on both ends. Additionally, a full-bridge sub-module MMC can address this issue but incurs additional loss because a half-bridge sub-module MMC lacks the capacity to ride through faults [7], [8].

The current source converter, which is the dual form with the voltage source converter, can realize flexibly adjustment of output dc voltage from zero to line voltage and controllable power factor [9]. It has obtained engineering application in the aspect of motor drive [10] and the compensation of reactive power [11] in the middle and low voltage fields. Maximum peak value of CSC valve voltage has not had enough attention because a few series devices are needed in the field of medium and low voltage grade.

The progress of IGCT provides strong support for development of this technology [12], [13]. The CSC consists of RB-IGCTs, has no commutation failure, so the inverter of the LCC-HVDC could be upgraded to CSC to improve reliability of the inverter grid. Also, the converters have the same characteristics, so LCC-CSC HVDC system has the ability of power reversal, fault ride-through and reducing DC voltage operation.

Reference [14] proposed the control method of interconnection between offshore wind farm and power grid based on current source converter, and can realize decoupling of active power and reactive power according to wind speed. In order to reduce additional loss caused by the bypass operation of the converter, the modulation index in the control technique is set as 1, to reduce dc current to reduce converter loss. In [15], the paper proposes cascade CSC is used to solve the problem of grid connection with offshore wind farms, reducing volume and cost of offshore converter stations. Similarly, in order to decrease loss of converter, a control scheme of minimum DC current is proposed. Although reducing DC current can

Manuscript received January 7, 2022; revised May 27, 2022; accepted July 7, 2022. Date of online publication June 27, 2023; date of current version August 17, 2023. This work was supported in part by Science and Technology Project of State Grid Corporation of China (5500202058059A0000).

W. W. Zhang, L. Qi, and K. Ji are with North China Electric Power University, Beijing 102206, China.

L. L. Chen, X. G. Wei (corresponding author, email: weixg366@163.com), C. Gao, and Z. Y. He are with China Electric Power Research Institute, Beijing 102209, China.

DOI: 10.17775/CSEEJPES.2022.00190

weaken problems caused by bypass operation to some extent: such as extra loss and lower power transmission efficiency, these problems cannot be fundamentally solved. The steady-state low frequency model of PWM-CSC in d-q coordinate system is derived in [16]. The control strategy of startup, power reversal and AC/DC fault is designed, which verifies feasibility of application of LCC-CSC system in the field of long-distance and large power capacity HVDC transmission system. Moreover, large inductance on DC side of CSC can provide natural protection against short-circuit faults [17], reducing stress on the converter. The theoretical derivation of power operating range is given in combination with steady-state model of PWM-CSC in [18], [19], but it is not further analyzed with the control technique of the system. Control strategy under unbalanced grid and dc fault ride through of CSC are proposed in [20] and [21], respectively. The system control strategy is more complicated due to the second-order circuit in the AC-side of the PWM-CSC. Control strategies in [14]–[16], [18], [19] are all affected by system parameters and cannot be adjusted through feedback.

In this paper, the working principle of CSC is analyzed. It is found peak valve voltage of the converter is high and voltage ripple ratio on the DC side is large due to the appearance of bypass operation during normal operation of CSC, resulting in a large amount of RB-IGCTs required and the big value of dc choke. Although fundamental frequency modulation method can solve these issues, DC voltage and reactive power are coupled [22], [23]. By proposing an improved modulation method in this paper, the occurrence of bypass during converter operation can be eliminated, the number of devices in series can be reduced by 31.5% under unity power factor operation, and the value of dc choke can be reduced by about 78.6%. Moreover, active power and reactive power operating range are derived according to the proposed modulation methods and the power factor is given when DC current and modulation in q-axis changes. Finally, effectiveness of the improved modulation method is verified, and active power and reactive power operating range is compared by simulations in PSCAD/EMTDC.

The remainder of this paper is organized as follows: Section II introduces the topology and operation mode of LCC-CSC HVDC system first, and then analyses valve voltage characteristic of PWM-CSC and its issues when applied in HVDC system. Section III proposes an improved modulation method that can solve the issues of PWM-CSC analyzed in Section II, then a control strategy of the system is derived which is insensitive to system parameters. Finally, active power and reactive power operating range is derived, and power factor is given combining with the control strategy of the system. Section IV gives simulation verification of the theoretical analysis. Conclusions are drawn in Section V.

II. Operation Mode of LCC-CSC HVDC and Valve Voltage Characteristic of PWM-CSC

A. Circuit Topology of LCC-CSC HVDC

The standard LCC-HVDC transmission system rectifier structure is adopted in the LCC-CSC HVDC system depicted in Fig. 1, including 12-pulse thyristor converters, compensation of reactive power, and filter equipment.

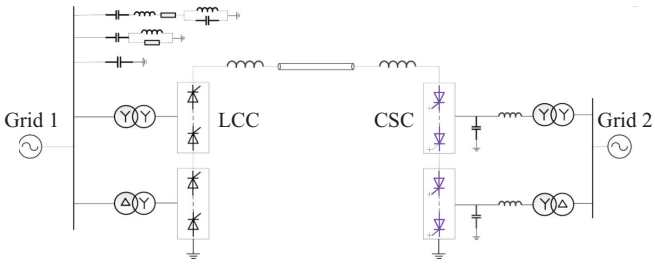

Fig. 1. Circuit topology of LCC-CSC HVDC system.

The inverter side is composed of two CSCs in series, topology of a single converter is shown in Fig. 2, and taking a single converter as an example to analysis the operating principle. RB-IGCTs make up the bridge legs of the converter. On the grid side, there is a second-order filter circuit composed of capacitors and inductors. The parallel connection of the filter capacitors benefits current commutation and filters out converter harmonics.

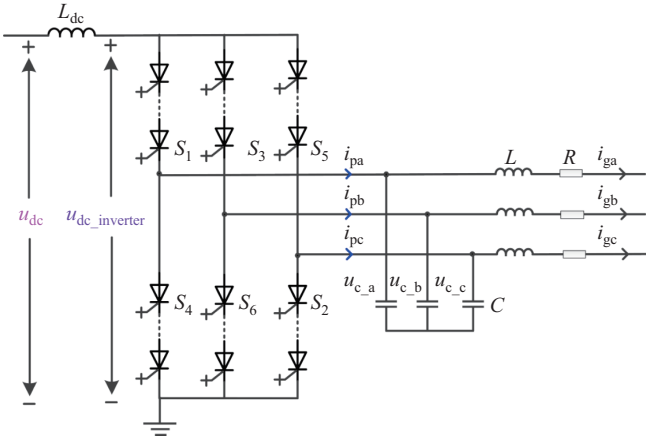

Fig. 2. Topology of current-source converter.

B. Operating Mode of LCC-CSC HVDC System

1) Operating Mode of System

The rectifier usually adopts minimum trigger angle control mode and DC current control model, and DC voltage and reactive power control modes in inverter side are usually employed in LCC-CSC HVDC system. Steady-state characteristics are shown in Fig. 3. In order to deal with voltage drop on the rectifier side, the inverter side can change to DC current control mode, corresponding to EF segment.

2) Operating Mode of PWM-CSC

The switching function and constraints of PWM-CSC can be derived in (1) and (2).

$$g_{\mathrm{j(j=a,b,c)}} = \begin{cases} 1 & \text{upper switch on and lower switch off} \\ 0 & \text{both switch on or off} \\ -1 & \text{upper switch off and lower switch on} \end{cases} \tag{1}$$

$$g_{\mathrm{a}} + g_{\mathrm{b}} + g_{\mathrm{c}} = 0 \tag{2}$$

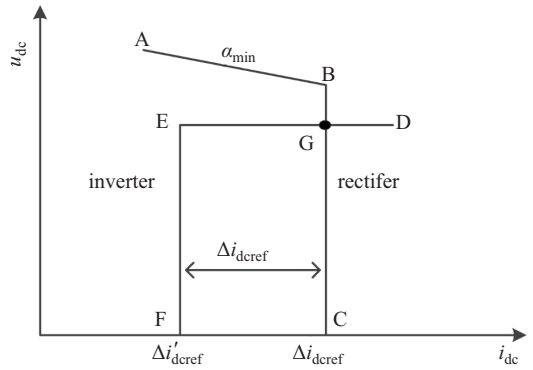

Fig. 3. Steady-state control scheme based on LCC-CSC HVDC system.

C. Valve Voltage Characteristic of PWM-CSC

There are only allowed two bridge legs conducting during operation of the converter According to (1) and (2), so they correspond to two working conditions:

i) the upper and lower bridge legs in different phases are on. Valve voltage of the converter is the filter capacitor line-voltage of the corresponding phases according to (1) and (2) and Fig. 2.

ii) The upper and lower bridge legs in the same phase are on. Valve voltage of the converter is zero. This operation mode is referred as bypass operation.

The waveform of converter valve voltage is shown in Fig. 4. $u_{\rm ab}$, $u_{\rm bc}$, $u_{\rm ca}$ are line-voltage of the filter capacitor, $U_{\rm dc}$ is the DC voltage of the system, $u_{\rm dc\_inverter}$ is the valve voltage of the converter. It can be seen from Fig. 4 that when PWM modulation method is used, valve voltage of converter is the jump value between filter capacitors line-voltage and zero voltage.

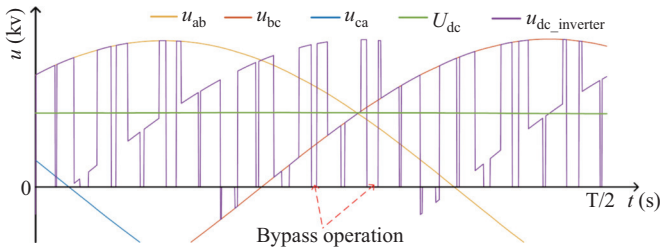

Fig. 4. DC voltage of the system, valve voltage of converter and filter capacitor line voltage working waveform.

D. Issues Analysis of PWM-CSC When Applied in HVDC System

1) High Peak Valve Voltage of the Converter

CSC operates with tri-logic signals, and it needs to ensure that only two bridge legs are in conduction state during operation. Therefore, bi-logic signals is often transforms into tri-logic signals through (3) [21].

$$\begin{bmatrix} g_{\rm a} \\ g_{\rm b} \\ g_{\rm c} \end{bmatrix} = \frac{1}{2} \begin{pmatrix} 1 & -1 & 0 \\ 0 & 1 & -1 \\ -1 & 0 & 1 \end{pmatrix} \begin{bmatrix} p_{\rm a} \\ p_{\rm b} \\ p_{\rm c} \end{bmatrix} \tag{3}$$

where $p_{\rm a}$, $p_{\rm b}$, $p_{\rm c}$ are the bi-logic signals. It can be seen from (3) when the bi-logic signals are $(1, 1, 1)$ or $(-1, -1, -1)$, the corresponding tri-logic signals are (0, 0, 0), and there will be the bypass operation. According to Fig. 4, the DC voltage of the system is the average value of the converter valve voltage. Therefore, the longer the bypass operation exists in a working cycle, the higher peak valve voltage of the converter will be, resulting in increase of the number of RB-IGCTs required and cost of the converter.

2) High Ripper Voltage Ratio

Valve voltage of the converter is the jump value between the filter capacitors line-voltage and zero voltage, therefore, the range of voltage fluctuation is wide. To keep the voltage ripper ratio of the transmission line satisfying the requirement of the HVDC system, a large dc choke should be chosen according to (4).

$$L_{\rm dc} = \frac{U_{\rm d(n)}}{n\omega I_{\rm dc} \times \frac{I_{\rm dc(n)}}{I_{\rm dc}}} \tag{4}$$

where $U_{\rm d(n)}$ is the RMS of the lowest characteristic harmonic voltage at DC side, $I_{\rm dc}$ is the rated dc current, $I_{\rm dc(n)}/I_{\rm dc}$ is the allowable relative value of the lowest characteristic harmonic current at DC side. n is the lowest characteristic harmonic. A large dc choke can decrease the voltage ripper and current ripper, but also will increase loss of active power and difficulty of engineering application.

In summary, those issues analyzed above will exist when PWM-CSC is applied in HVDC system. Therefore, advanced modulation methods are needed to solve these issues.

III. Improved Control Strategy and Its Power Operating Range

To solve these existing issues, analyzed in Section II, this section proposes an improved modulation method. At present, modulation methods used in CSC are mainly divided into two categories: on-line modulation methods [24] and off-line modulation methods [25], [26]. Off-line modulation methods need to store data in advance, so it is difficult to satisfy the requirements of power systems under complicated working conditions. On-line modulation methods mainly include SPWM and SVPWM. SPWM methods have the advantages of simple control and easy hardware implementation, so it has been widely used.

A. The Improved Modulation Method of CSC

As analyzed in Section II, it is the bypass operation that results in valve voltage of the converter being the jump value between the filter capacitor line-voltage and zero voltage, therefore, no bypass operation modulation method should be proposed to fundamentally solve these existing issues.

It can be seen from (3) there will be the bypass operation when the bi-logic signals are $(1, 1, 1)$ or $(-1, -1, -1)$. Therefore, taking SPWM as an example, when the modulation index is less than 1, the converter will be bypassed once in half a carrier cycle. In order to avoid the bypass operation, the modulation method of the converter should satisfy the following requirements:

i) The modulation index is greater than 1.

ii) The carrier is only compared with two carriers in half a period;

iii) In order to ensure symmetry of single-phase waveform, the number of carriers in a period should be odd.

iv) In order to ensure symmetry of three-phase waveform, frequency of a single carrier should be divisible by 120.

Carrier frequency satisfying the above requirements is 150 Hz, 450 Hz, *et al*. When carrier frequency is 150 Hz, the corresponding tri-logic signals are square wave, and the system will lose the ability to adjust reactive power. When the carrier frequency is 450 Hz, there will be two situations, but only one situation without bypass operation is shown in Fig. 5.

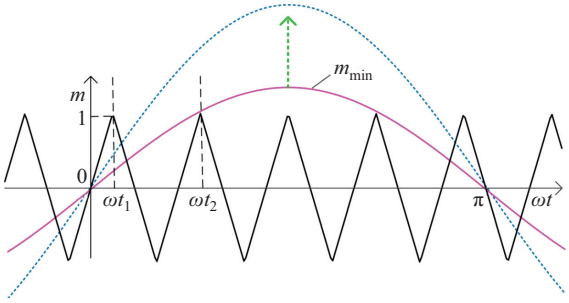

Fig. 5. Proposed modulation method of CSC.

In order to ensure the modulation index always satisfies the requirements of the modulation method when it changes during steady-state, the modulation index is limited as $m(\omega t_1) > 1$ and $m(\omega t_2) < 1$. The three-phase sinusoidal modulation method and the bi-logic and tri-logic signals are shown in Fig. 6. At this time, switch signals of the upper bridge legs are completely complementary, and switch signals of the same phase do not have overlap.

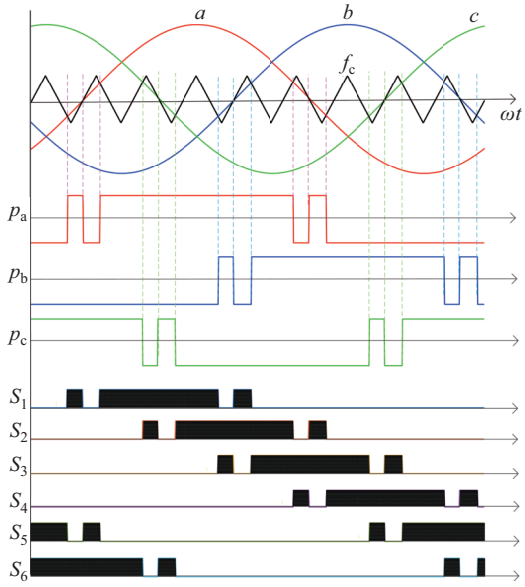

Fig. 6. Modulation method and trigger signal of PWM-CSC.

The improved modulation method operates in the over modulation region, and the relationship between the modulation index and the effective value of the fundamental current is shown in Fig. 7 according to constraint of the improved modulation.

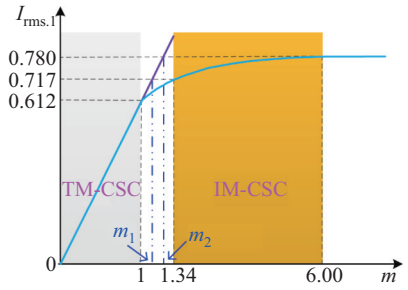

Fig. 7. The relationship between the modulation index and the effective value of the fundamental current.

As can be seen from Fig. 7, variation range of fundamental current of the improved modulation method is adjustable compared with the fundamental frequency modulation method. What is more, the improved modulation method does not have the bypass operation, avoiding high peak valve voltage and wide ratio of DC current ripper compared to traditional modulation methods.

B. The Improved Control Strategy of LCC-CSC HVDC System

The second-order filter circuit on the grid side of the CSC makes the control scheme more complicated, and it is difficult to achieve inner and outer loop fast control strategy similar to VSC. In [14]–[16], [18], [19], the relationship between grid-current and converter-current is obtained by establishing the expression of steady-state circuit. This expression relying on circuit parameters are easily affected by system parameters.

The equivalent d-q circuit of CSR is analyzed in [27], the equivalent circuit shown in Fig. 8 of LCC-CSC HVDC system when grid-voltage phase-locked loop(PLL) is employed.

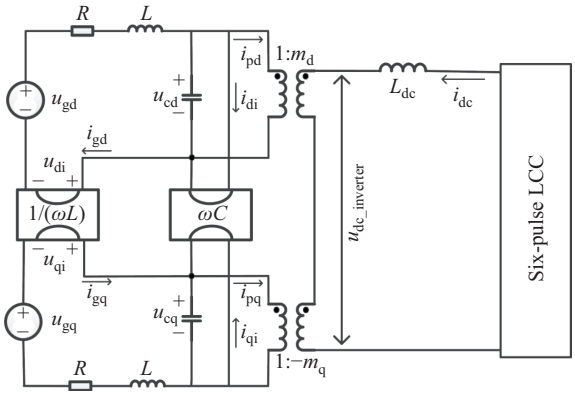

Fig. 8. D-Q equivalent circuit of LCC-CSC HVDC system.

According to Fig. 8, we can obtain the following equations:

$$\begin{cases} L\dfrac{\mathrm{d}i_{\mathrm{gd}}}{\mathrm{d}t} = u_{\mathrm{cd}} - u_{\mathrm{gd}} + \omega L i_{\mathrm{gq}} - R i_{\mathrm{gd}} \\ L\dfrac{\mathrm{d}i_{\mathrm{gq}}}{\mathrm{d}t} = u_{\mathrm{cq}} - u_{\mathrm{gq}} - \omega L i_{\mathrm{gd}} - R i_{\mathrm{gq}} \end{cases} \tag{5}$$

$$\begin{cases} C\dfrac{\mathrm{d}u_{\mathrm{cd}}}{\mathrm{d}t} = i_{\mathrm{pd}} - i_{\mathrm{gd}} + \omega C u_{\mathrm{cq}} \\ C\dfrac{\mathrm{d}u_{\mathrm{cq}}}{\mathrm{d}t} = i_{\mathrm{pq}} - i_{\mathrm{gq}} - \omega C u_{\mathrm{cd}} \end{cases} \tag{6}$$

Set $\mathrm{d}X/\mathrm{d}t = 0$ in steady-state, so grid-current and capacitor-voltage in d-q component can be obtained:

$$\begin{cases} u_{\mathrm{cd}} = \dfrac{u_{\mathrm{gd}} - \omega L i_{\mathrm{pq}}}{1-\omega^2 LC} \\ u_{\mathrm{cq}} = \dfrac{\omega L i_{\mathrm{pd}} + u_{\mathrm{gq}}}{1-\omega^2 LC} \end{cases} \tag{7}$$

$$\begin{cases} i_{\mathrm{gd}} = \dfrac{\omega C u_{\mathrm{gq}} + i_{\mathrm{pd}}}{1-\omega^2 LC} \\ i_{\mathrm{gq}} = \dfrac{i_{\mathrm{pq}} - \omega C u_{\mathrm{gd}}}{1-\omega^2 LC} \end{cases} \tag{8}$$

At this time, the expression of DC voltage and reactive power are as follows setting $u_{gq} = 0$:

$$\begin{aligned} u_{\mathrm{dc}} &= \frac{3}{2}(m_{\mathrm{d}} u_{\mathrm{cd}} + m_{\mathrm{q}} u_{\mathrm{cq}}) \\ &= \frac{3}{2}\cdot\frac{m_{\mathrm{d}} u_{\mathrm{gd}} - m_{\mathrm{d}}\omega L i_{\mathrm{pq}} + m_{\mathrm{q}}\omega L i_{\mathrm{pd}}}{1-\omega^2 LC} \\ &= \frac{3}{2}\cdot m_{\mathrm{d}}\left(u_{\mathrm{gd}} + \omega L\frac{-\frac{2}{3}Q_{\mathrm{ac}}}{u_{\mathrm{gd}}}\right) + m_{\mathrm{q}}\omega L\frac{\frac{2}{3}P_{\mathrm{ac}}}{u_{\mathrm{gd}}} \end{aligned} \tag{9}$$

$$Q_{\mathrm{ac}} = -\frac{3}{2}u_{\mathrm{gd}} i_{\mathrm{gq}} = \frac{3}{2}\cdot\frac{\omega C u_{\mathrm{gd}}^2 - \frac{P_{\mathrm{ac}}}{U_{\mathrm{dc}}}u_{\mathrm{gd}} m_{\mathrm{q}}}{1-\omega^2 LC} \tag{10}$$

DC voltage u_{dc} and reactive power Q_{ac} can be expressed as $u_{\mathrm{dc}} = f(m_{\mathrm{d}}, m_{\mathrm{q}}, P_{\mathrm{ac}}, Q_{\mathrm{ac}})$ and $Q_{\mathrm{ac}} = f(P_{\mathrm{ac}}, m_{\mathrm{q}})$ according to (9) and (10). Active power P_{ac} and Q_{ac} are the reference values given by the system, so U_{dc} is the known quantity under the control strategy of constant current at the rectifier side. Therefore, DC voltage is related to m_{d} and m_{q}, while reactive power is related to m_{q} and DC current. For the control system, changing DC current and m_{q} will change reactive power of the system. When m_{q} is known, changing m_{d} to keep the DC voltage adjustable, m_{d} and m_{q} can be obtained through (11).

$$\begin{cases} m_{\mathrm{d}} = m\cos(\varphi_1 - \varphi_2) \\ m_{\mathrm{q}} = m\sin(\varphi_1 - \varphi_2) \end{cases} \tag{11}$$

where φ_1 is the phase angle of grid-voltage, φ_2 is phase angle of modulation function of converter, m is modulation index of the converter.

The control scheme of LCC-CSC HVDC system composed of LCC and PWM-CSC is shown in Fig. 9 according to (9) and (10).

C. Power Operating Range Under Different Modulation Methods

1) Operating Range of Reactive Power Under Different Modulation Methods

Assuming DC current is kept constant when analyzing the power operating range, (12) can be obtained.

$$\begin{cases} m_{\mathrm{d}} = \dfrac{i_{\mathrm{pd}}}{i_{\mathrm{dc}}} \\ m_{\mathrm{q}} = \dfrac{i_{\mathrm{pq}}}{i_{\mathrm{dc}}} \end{cases} \tag{12}$$

Substitute (12) into (9) and (10), active power and reactive power can be derived under the steady-state.

$$P_{\mathrm{ac}} = \frac{3}{2}\cdot\frac{u_{\mathrm{gd}} m_{\mathrm{d}}}{1-\omega^2 LC} i_{\mathrm{dc}} \tag{13}$$

$$Q_{\mathrm{ac}} = \frac{3}{2}\cdot\frac{\omega C u_{\mathrm{gd}}^2 - i_{\mathrm{dc}} u_{\mathrm{gd}} m_{\mathrm{q}}}{1-\omega^2 LC} \tag{14}$$

PWM-CSC can realize the decoupled operating of active power and reactive power within a certain operating range. However, due to limitations such as: modulation index, current and voltage of the converter, it will show power coupling in a certain range. It can be seen from (14) reactive power is linked with the m_{q}, m_{q} is as follows:

$$-\sqrt{m_{\max}^2 - m_{\mathrm{d}}^2} \le m_{\mathrm{q}} \le \sqrt{m_{\max}^2 - m_{\mathrm{d}}^2} \tag{15}$$

Steady-state working point is shown in Fig. 10. The range of reactive power in the system is proportion to the change of m_{q} according to (14). Limited by the upper and lower limits of modulation index, the change range of m_{q} is narrow. $+\Delta m_{\mathrm{q}}$ and $-\Delta m_{\mathrm{q}}$ affect the value of reactive power absorbed and generated by the system, respectively. In this range, active power and reactive power are decoupled. When the upper or lower limits of the modulation index are reached, the steady-state operation point will move along the boundary of the circle, so active power and reactive power are coupled.

According to the operating range of m_{d} and m_{q}, the power operating range of CSC under the improved modulation method can be obtained, as shown in Fig. 11. In Fig. 11, L_1, L_2, L_3, L_4 are modulation constraints.

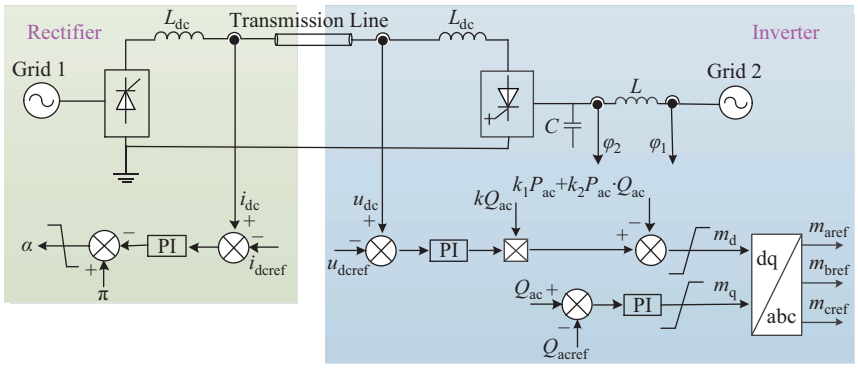

Fig. 9. Control scheme for LCC-CSC HVDC transmission system.

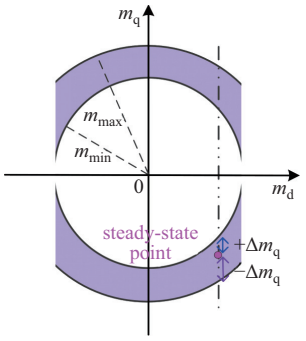

Fig. 10. Operating range of m_d and m_q.

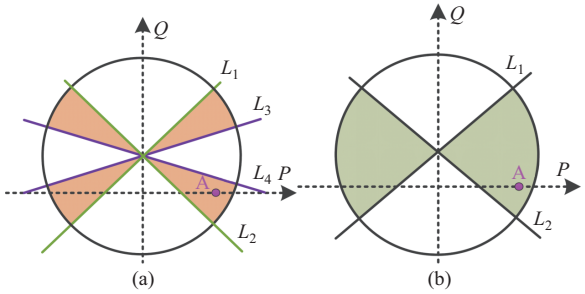

Fig. 11. Active power and reactive power operating range of different modulation methods. (a) Power operating range of improved modulation method. (b) Power operating range of traditional modulation method.

Figure 11(a) shows the power operating range of the CSC under the improved modulation method. According to analysis in Section III, the operating range of reactive power is narrow due to the limiting modulation index. Fig. 11(b) shows the power operating range of the CSC under traditional modulation methods. Theoretically, the variable range of modulation index is wider than of the traditional modulation method, and the operating range of reactive power is large. However, the following two points limit the power operating range of the CSC.

i) CSC will cause bypass operation after adopting traditional modulation method, therefore, in order to reduce peak voltage withstand by the converter, the converter should operate at a high index in the steady state, which limits the ability of the converter to generate reactive power.

ii) When the modulation index decreases, not only the harmonic distortion rate will increase, but also the duration of the bypassed operation will be longer. DC voltage of the current source converter is supported by filter capacitor voltage, in order to ensure stability of the DC voltage, the intercepted filter capacitor voltage will move up, leading to a higher peak valve voltage.

The above two points correspond to the ability of the converter to generate and absorb reactive power, and the constraints of the two are contradictory. Therefore, the reactive power operating range of the converter under the traditional modulation method needs to be considered in combination with the peak valve voltage of the converter.

2) Operating Range of Active Power Under the Different Modulation Methods

Active power and reactive power remain decoupled during change of reactive power when the inverter adopts constant voltage mode. However, when active power changes, there are decoupling intervals and coupling intervals between active power and reactive power. The expression of active power at inverter side is as (16):

$$P_{\rm ac} = u_{\rm dc} \cdot i_{\rm dc} \tag{16}$$

The change of active power of LCC-CSC HVDC system is mainly realized by adjusting DC current. In order to maintain stability of reactive power, $m_{\rm q}$ needs to be adjustment to compensate variation of active power according to (10). It can be seen from (10) that when the product of $m_{\rm q}$ and $P_{\rm ac}$ remain unchanged, active power and reactive power are decoupled. When $m_{\rm q}$ reaches its limitation, they will be coupling.

Reactive power can be expressed as (17).

$$Q_{\rm ac} = \frac{3\omega C u_{\rm gd}^2}{2(1-\omega^2 LC)} - \frac{3}{2} \cdot \frac{u_{\rm gd} m_{\rm q}}{(1-\omega^2 LC) U_{\rm dc}} \cdot P_{\rm ac} \tag{17}$$

Limitation of the maximum modulation index of CSC causes the coupling of active power and reactive power according to (17). When active power of the system is less than $P_{\rm lim}$, CSC cannot keep reactive power being zero, and CSC cannot operate at unity power factor. Therefore, the expression of $P_{\rm lim}$ is (18):

$$P_{\rm lim} = \frac{\omega C u_{\rm gd} U_{\rm dc}}{m_{\rm q}} \tag{18}$$

When $m_{\rm q}$ reaches maximum value, $P_{\rm lim}$ reaches minimum value according to (18). If decreasing active power continuously, the converter cannot operate at unity power factor by adjusting $m_{\rm q}$.

Regulation of active power and reactive power of the converter are realized by changing DC current and $m_{\rm q}$, separately. Therefore, in the process of power change, the relationship between the power factor at the converter and DC current and $m_{\rm q}$ is shown in Fig. 12 according to (17) and (18).

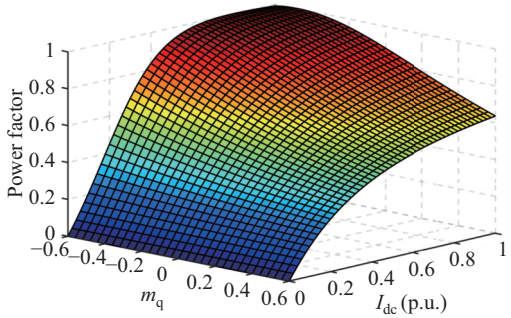

Fig. 12. Power factor at the grid side of PWM-CSC.

To sum up, when DC current is greater than $I_{\rm lim}$, the converter can operate at unity power factor according to Fig. 12. When DC current is less then $I_{\rm lim}$, the converter cannot operate at unity power factor, and the power factor decreases with decrease of DC current.

IV. Simulation Results of LCC-CSC HVDC System

In order to verify effectiveness of the control strategy and correctness of operating range of power, a monopole simulation model depicted in Fig. 1. was built in PSCAD/EMTDC. Simulation parameters are shown in Tables I and II.

TABLE I
DC Side Parameters Of LCC-CSC HVDC Transmission Syatem

Parameters	Value
Rated power	1000 MW
DC voltage DC current	500 kV 2 kA
Equivalent resistance of transmission line	5 Ω
Equivalent capacitor of transmission line	26 μF
Equivalent inductance of transmission line	0.6 H

TABLE II
CSC Side Parameters Of LCC-CSC HVDC Transmission Syatem

Parameters	Improved inverter side	Traditional inverter side
Grid-voltage	500 kV	500 kV
Transformer ratio	500 kV/185 kV	500 kV/240 kV
Inductor of LC filter	23 μF	14 μF
capacitor of LC filter	90 mH	130 mH
DC choke	0.3 H	1.2 H
Carrier frequency	450 Hz	450 Hz
RB-IGCT switch frequency	150 Hz	450 Hz

A. Start-up Process and Steady-state of LCC-CSC HVDC System

The startup's transient process is depicted in Fig. 13. Both ends of the converter are locked during the time interval of 0–0.4 s. At 0.4 s, both converter stations are unlocked simultaneously, rectifier side current climbs to 2 kA in 0.2 s at a fixed gradient, and the inverter side voltage rises to 500 kV in 0.2 s. There is a small overshoot of DC voltage, about 4%, throughout the growing process of DC voltage and DC current. After a brief period of transition, the DC voltage and DC current stay constant, and their fluctuation range satisfies specifications. Active power and reactive power of the inverter side remain stable, and unity power factor operation of the system is realized.

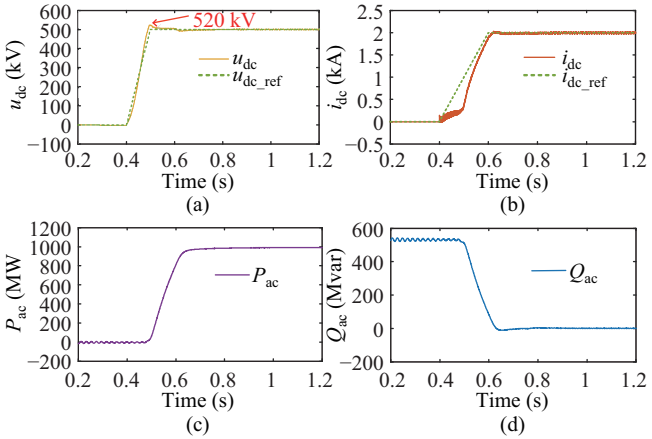

Fig. 13. Startup transient of LCC-CSC HVDC system. (a) DC voltage. (b) DC current. (c) Active power at the grid side of PWM-CSC. (d) Reactive power at the grid side of PWM-CSC.

B. Effectiveness Analysis of the Improved Modulation Method

In order to verify improvement of key issues of the PWM-CSC after adopting the improved modulation method, comparisons are made between the traditional modulation method and the improved modulation method based on circuit topology shown in Fig. 1. Traditional inverter side parameters are shown in Table I, rectifier side parameters are unchanged.

1) Comparisons of the Valve Voltage of the Converter

In Section III, the relationship between peak voltage and reactive power of the converter is analyzed. In order to make a balance between valve voltage of the converter and reactive power, the modulation index in steady-state of the converter under the traditional modulation method is set at 0.93 by adjusting system parameters, and under the improved modulation method is 2.13.

Valve voltage of the low voltage converter waveform under the traditional modulation method and the improved modulation method are shown in Fig. 14. According to analysis of the working principle of the converter, the traditional modulation method has bypass operation and then valve voltage of the converter will be zero. Therefore, to ensure the same DC voltage grade of the system, peak voltage withstood by the converter will be higher, about 1.656 times the DC voltage of the system. However, the improved modulation method could avoid bypass operation, so peak voltage withstood by the converter is lower, about 1.132 times the DC voltage of the system.

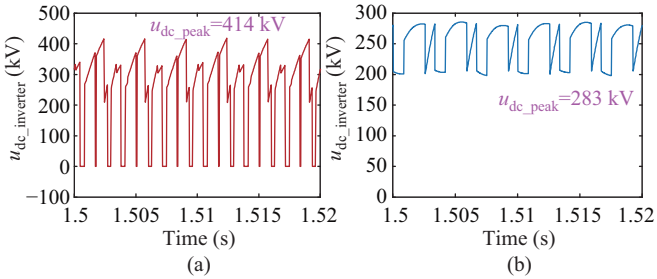

Fig. 14. Valve voltage of the PWM-CSC adopted different modulation methods. (a) Traditional modulation method. (b) Improved modulation method.

The rated voltage of RB30QY4500IGCT is 4500 V. Taking half of the rated voltage of RB-IGCT as operation voltage, the improved modulation method can save 31.5% of total devices compared with traditional modulation method in unity power factor operation, which greatly reduces cost of the converter.

2) Relationship Between Dc Current Ripper Ratio and the Dc Choke

When PWM-CSC is applied to HVDC system, due to the particularity of PWM-CSC working principle, the different values of the two ends converters fluctuate greatly under the traditional modulation method, resulting in high current ripper ratio. In order to decrease dc current ripper ratio, a large value of dc choke must be chosen. DC current waveforms under different dc chokes are shown in Fig. 15.

DC current ripper ratio cannot satisfy the requirement of the system by choosing a small value of the dc choke according to Fig. 15(a), (b), (c). The dc current ripper ratio is about

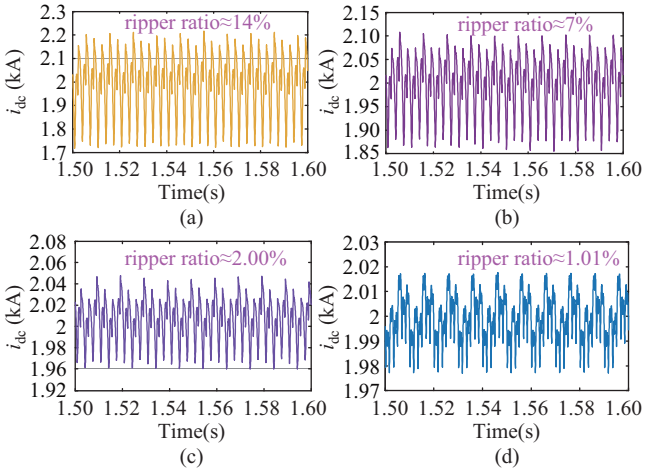

Fig. 15. DC current waveforms under different values of dc choke. (a) The value of dc choke is 0.3 H under the traditional modulation method. (b) The value of dc choke is 0.9 H under the traditional modulation method. (c) The value of dc choke is 1.2 H under the traditional modulation method. (d) The value of dc choke is 0.3 H under the improved modulation method.

2.00% when the dc choke value increased to 1.2 H. However, a large value of dc choke may bring about more power loss and slow response speed of the system. After adopting the improved modulation method, the dc current ripper ratio is about 0.70% with the dc choke value at 0.3 H as shown in Fig. 15(d). Therefore, the value of the dc choke can decrease by 78.6% compared to the traditional modulation method.

3) Grid-voltage and Grid-current

Switching frequency of the RB-IGCT is 150 Hz under the improved modulation method, and switching frequency is 450 Hz under the traditional modulation method. The distortion rate of grid side current waveform is closely related to switching frequency of devices and the ripple coefficient of DC current. Waveforms of the grid-voltage and grid-current are shown in Fig. 16.

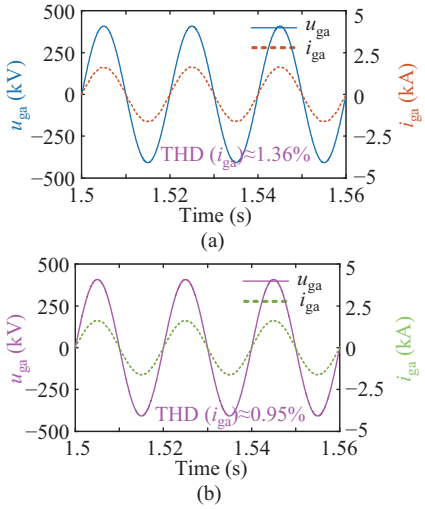

Fig. 16. Voltage and current waveforms of grid side. (a) Adopting the traditional modulation method. (b) Adopting the improved modulation method.

Although switching frequency of the devices under the traditional modulation method is higher, which is three times that of the improved modulation method, the ripple coefficient of DC current under the traditional modulation method is higher than of improved modulation, so total harmonic distortion (THD) of grid-current is higher than under the improved modulation method according to Fig. 16.

THD of grid-current and DC ripper ratio under different values of dc choke of traditional modulation method are shown in Table III. It can be seen from Tables I, II and III when the resonant frequency of LC parameters are close, THD of grid-current in CSC is mainly affected by DC ripple ratio.

TABLE III
DC CURRENT RIPPER RATIO AND THD OF GRID-CURRENT UNDER DIFFERENT VALUE OF DC CHOKE

Value of dc choke	DC current ripper ratio	THD of grid-current
0.3H	6.60%	1.57%
0.9H	3.50%	1.43%
1.2H	2.00%	1.36%

In conclusion, compared with the traditional modulation method, the converter with the improved modulation method has the following advantages:

i) Under the improved modulation method, peak valve voltage is 68.5% of the peak voltage of the traditional modulation method, which can significantly reduce the number of bridge leg devices in series, reduce difficulty of series voltage sharing and cost of converter valve.

ii) The improved modulation method does not have bypass operation, so the ripple ratio of DC current is small. The ripple ratio of DC current is only 0.70% after choosing the value of dc choke as 0.3 H. The DC current ripple ratio is about 2.00% when the 1.2 H dc choke was chosen under the traditional modulation method.

iii) When the resonant frequency of LC parameters is close, the THD of grid-current is mainly affected by DC current ripple ratio. Therefore, the THD of grid-current under the improved modulation method is smaller.

C. Verification of Operating Range of Reactive Power

The improved modulation method can avoid bypass operation and has adjustable modulation index. Modulation in d-axis and in q-axis may influence DC voltage and reactive power according to (9) and (10). To verify correctness of the reactive power operating range analysis, several simulations have been made.

Figures 17 and 18 are waveforms of active power and valve voltage of converter when the converter generates reactive power under traditional modulation method. It can be seen from Fig. 17 and 18 when reactive power changes, active power basically remains unchanged. During steady-state operation, the modulation index of the traditional modulation method is 0.93. When the modulation index increases to 1, voltage amplitude of the filter capacitors at the grid side increases, and the converter generates reactive power, with an upper limit of 146 Mvar. By decreasing the modulation index, amplitude of filter capacitors voltage decreases, and the converter absorbs reactive power. As the modulation index decreases, duration of the bypass operation increases, and due to the upper limit of filter capacitor voltage, the modulation

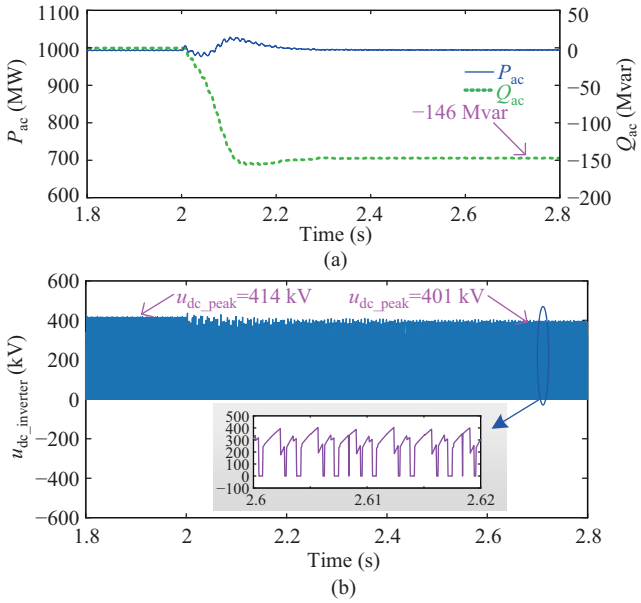

Fig. 17. Simulation results when CSC generates reactive power under traditional method. (a) Active power and reactive power. (b) The valve voltage of the converter.

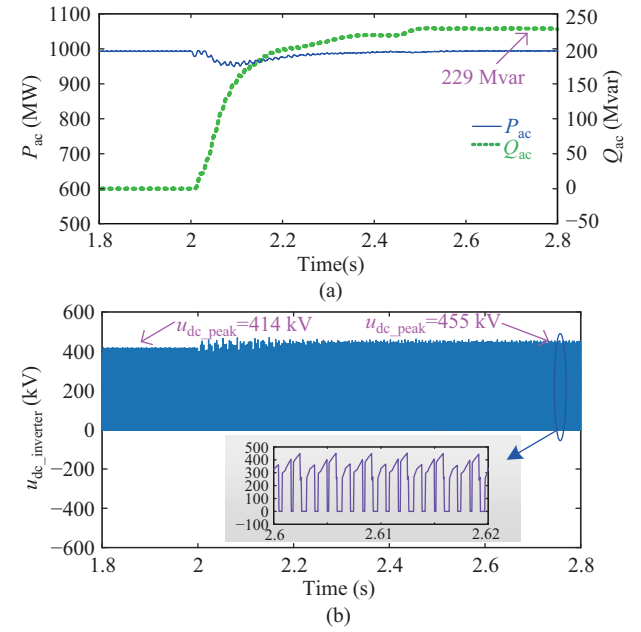

Fig. 18. Simulation results when CSC absorbing reactive power under traditional method. (a) Active power and reactive power. (b) The valve voltage of the converter.

index has a low limit on the premise of ensuring stability of DC voltage. When the modulation index is reduced to 0.85, the lower limit of reactive power absorbed by the converter is 229 Mvar.

Change of reactive power is accompanied by change of peak valve voltage according to Figs. 17(b) and 18(b). Peak valve voltage of the converter increases from 414 kV to 455 kV, an increase of about 10%, when the converter generates reactive power of 146 Mvar.

Figures 18 and 19 are waveforms of active power and valve voltage of converter when the converter changes reactive

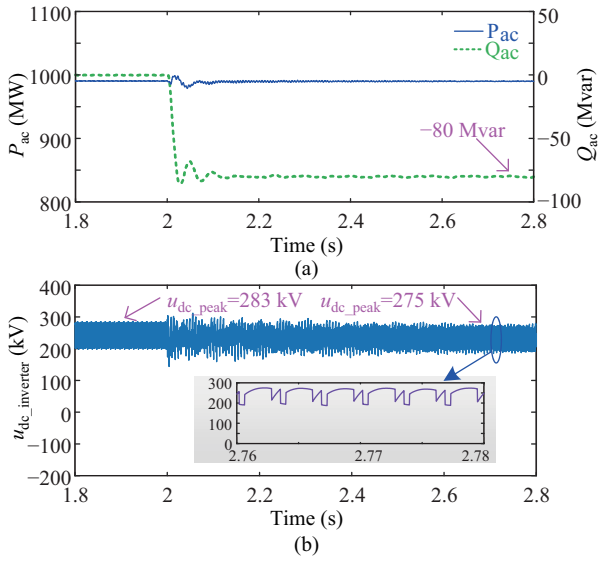

Fig. 19. Simulation results when CSC generates reactive power under improved method. (a) Active power and reactive power. (b) The valve voltage of the converter.

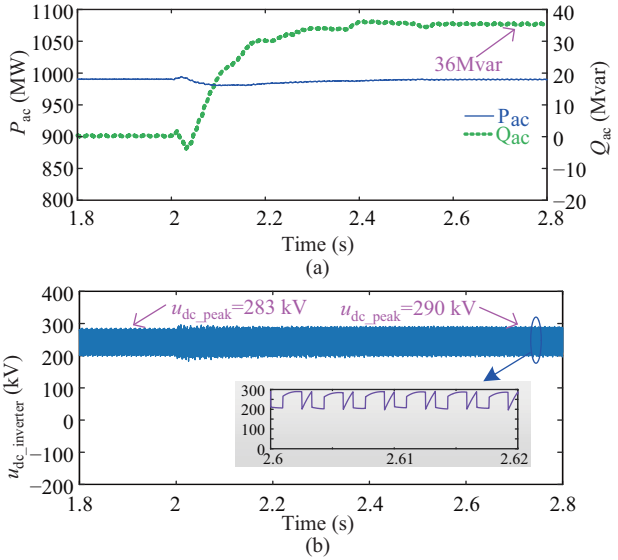

Fig. 20. Simulation results when CSC absorbing reactive power under improved method. (a) Active power and reactive power. (b) The valve voltage of the converter.

power under the improved modulation method. Since regulation range of the effective value of the fundamental current at the grid side is narrow, the operating range of reactive power is also relatively small compared to traditional modulation method. When upper and lower limits of the modulation ratio are reached, reactive power is −80 Mvar and 36 Mvar, respectively.

According to Figs. 19(b) and 20(b), when the converter reaches the limit of reactive power, peak valve voltage increases from 283 kV to 290 kV, an increase of only 2.47%.

To sum up, the CSC can change the reactive power and realize power decoupling on the premise of keeping active power unchanged within a certain range. The operating range of the reactive power of the converter under the traditional

modulation method is significantly larger than of the improved modulation method. When reactive power changes accompanied with peak valve voltage withstand by the converter changing, resulting in peak valve voltage increase. Under maximum generating reactive power, devices in series with improved modulation method can save 36.5% compared to traditional modulation method. Therefore, there should be a compromise between reactive power and valve voltage.

D. Verification of Operating Range of Active Power

1) Verification of Critical Power $p_{\rm lim}$ under different modulation methods

As the analysis of active power operating range in Section III, change of active power is realized by adjusting DC current, and there is a critical $P_{\rm lim}$ when active power changes. The position of $P_{\rm lim}$ is determined by the change range of modulation index. Fig. 21(a) and (b) are waveforms of critical power when DC current changes under the two modulation methods.

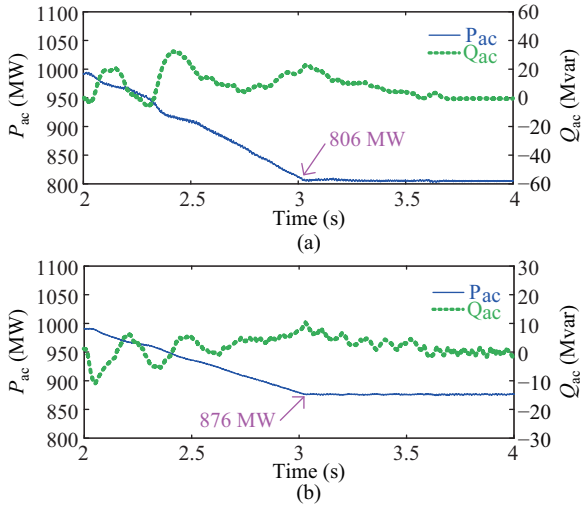

Fig. 21. Simulation results of critical power under different modulation methods. (a) Traditional modulation method. (b) Improved modulation method.

Reduce DC current linearly at 2 s. It can be seen from Fig. 21 after DC current gets stable, reactive power of the system can be kept at zero, so active power and reactive power are decoupled in this interval. Critical power $P_{\rm lim}$ under the traditional modulation method is 806 MW, which is 81.6% of rated active power. Therefore, the decoupling interval under the traditional modulation method accounts for 19.4% of rated power. Similarly, critical power $P_{\rm lim}$ under the improved modulation method is 876 MW, and the decoupling interval accounts for 12.4% of rated power. It can also be proved that critical point of $P_{\rm lim}$ under the traditional modulation strategy is smaller compared with the improved modulation method.

2) Verification of Operating Characteristics Under Different Modulation Methods

After reaching critical power $P_{\rm lim}$, if active power continues to be reduced, it can be seen from (17) that $m_{\rm d}$ and $m_{\rm q}$ remain unchanged at this time, so reactive power and active power change linearly in the process. Figs. 22 and 23 show

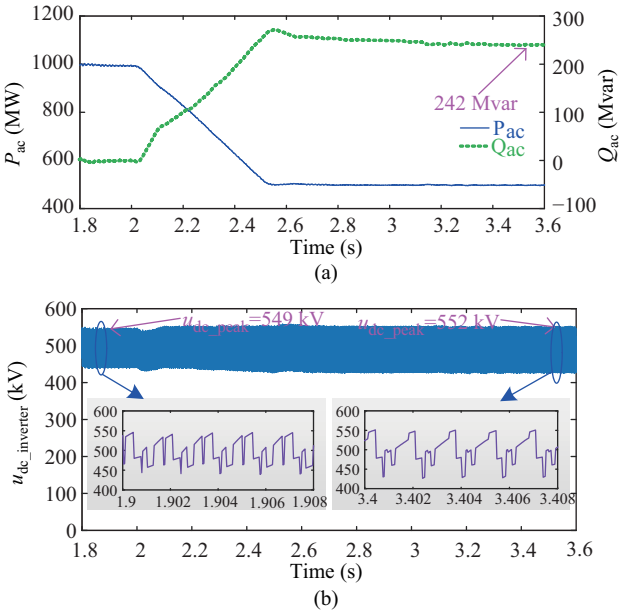

Fig. 22. Simulation results under the half load of the traditional modulation method. (a) Active power and reactive power. (b) Valve voltage of the converter.

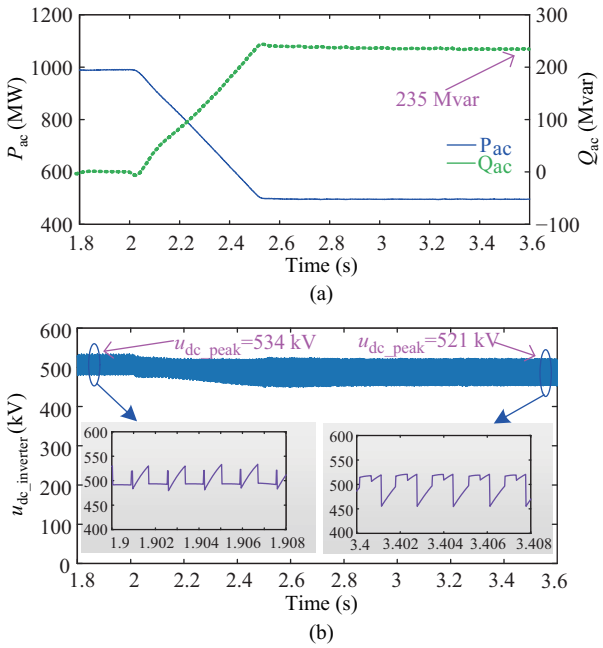

Fig. 23. Simulation results under the half load of the improved modulation method. (a) Active power and reactive power. (b) Valve voltage of the converter.

the waveforms of power and valve voltage of the converter under half load operation of the two modulation methods.

As we can be seen from Figs. 22 and 23, in the process of linear reduction of active power, reactive power increases linearly. This is because enough adjustable voltage cannot be generated on the filter capacitor when DC current decreases, the converter absorbs a certain amount of reactive power.

When active power is operating in half load, reactive power absorbed by the converter under the two modulation methods is approximately equal, and DC voltage remains unchanged

and change of peak voltage of the converter is small between rated power operation and half load power operation. Due to the constraint of the modulation index of the converter, there is a coupling interval between active power and reactive power, and the smaller active power is, the greater reactive power absorbs, which is very unfavorable. Therefore, a better system control strategy coordinating electrical quantities at two-terminals is needed to reduce dependence of reactive power on the grid-side.

V. Conclusion

Based on analysis of working principle of the PWM-CSC, several issues of PWM-CSC when applied in HVDC system are elaborated, such as high peak valve voltage of the converter and high voltage ripper ratio. These issues will bring about more RB-IGCTs in series and a large value of dc choke needed. To solve these issues, an improved modulation method is proposed. The improved modulation method can avoid bypass operation, so it can reduce the amount of the RB-IGCTs in series and value of the dc choke, about 31.5% and 78.6%, improving practicability of engineering application.

Operating range of active power and reactive power are derived under the traditional method and improved method of PWM-CSC, and the relationship of power factor, modulation in q-axis and DC current are given. Simulation results show reactive power operation of the converter under the improved modulation method is about one-third of that under the traditional modulation method, and power decoupling operating range is about 12.4% and 19.4%, respectively. However, after critical power $P_{\lim}$, the converter will have power coupling, and the relationship between reactive power and active power is linear.

References

[1] R. Blasco-Gimenez, N. Aparicio, S. Ano-Villalba, and S. Bernal-Perez, "LCC-HVDC connection of offshore wind farms with reduced filter banks," *IEEE Transactions on Industrial Electronics*, vol. 60, no. 6, pp. 2372–2380, Jun. 2013.

[2] N. Flourentzou, V. G. Agelidis, and G. D. Demetriades, "VSC-based HVDC power transmission systems: an overview," *IEEE Transactions on Power Electronics*, vol. 24, no. 3, pp. 592–602, Mar. 2009.

[3] S. M. Muyeen, R. Takahashi, and J. Tamura, "Operation and control of HVDC-connected offshore wind farm," *IEEE Transactions on Sustainable Energy*, vol. 1, no. 1, pp. 30–37, Apr. 2010.

[4] R. Zeng, L. Xu, L. Z. Yao, S. J. Finney, and Y. Wang, "Hybrid HVDC for integrating wind farms with special consideration on commutation failure," *IEEE Transactions on Power Delivery*, vol. 31, no. 2, pp. 789–797, Apr. 2016.

[5] H. Rao, Y. B. Zhou, C. Y. Zou, S. K. Xu, Y. Li, L. Yang, and W. H. Huang, "Design aspects of hybrid HVDC system," *CSEE Journal of Power and Energy Systems*, vol. 7, no. 3, pp. 644–653, May 2021, doi: 10.17775/CSEEJPES.2020.00980.

[6] G. Li, T. An, J. Liang, W. Liu, T. Joseph, J. J. Lu, M. Szechtman, B. R. Andersen, and Y. L. Lan, "Power reversal strategies for hybrid LCC/MMC HVDC systems," *CSEE Journal of Power and Energy Systems*, vol. 6, no. 1, pp. 203–212, Mar. 2020.

[7] H. Rao, G. Y. Li, R. B. Cao, W. H. Huang, and Y. Li, "Fault ride-through strategy of LCC-MMC hybrid multi-terminal UHVDC system," in *Proceedings of the 2019 IEEE 8th International Conference on Advanced Power System Automation and Protection (APAP)*, 2019, pp. 485–490.

[8] L. X. Hou, S. Q. Zhang, Y. D. Wei, X. Q. Li, and Q. R. Jiang, "A hybrid-arm modular multilevel converters topology with DC low voltage operation and fault ride-through capability for unidirectional HVDC bulk power transmission," *IEEE Transactions on Power Delivery*, vol. 35, no. 6, pp. 2812–2820, Dec. 2020.

[9] Y. Xiao, B. Wu, S. C. Rizzo, and R. Sotudeh, "A novel power factor control scheme for high-power GTO current-source converter," *IEEE Transactions on Industry Applications*, vol. 34, no. 6, pp. 1278–1283, Nov./Dec. 1998.

[10] J. C. Wiseman, B. Wu, and G. S. P. Castle, "A PWM current-source rectifier with active damping for high power medium voltage applications," in *Proceedings of the 2002 IEEE 33rd Annual IEEE Power Electronics Specialists Conference*, 2002, pp. 1930–1934.

[11] H. F. Bilgin, M. Ermis, K. N. Kose, A. Cetin, I. Cadirci, A. Acik, T. Demirci, A. Terciyanli, C. Kocak, and M. Yorukoglu, "Reactive-power compensation of coal mining excavators by using a new-generation STATCOM," *IEEE Transactions on Industry Applications*, vol. 43, no. 1, pp. 97–110, Jan./Feb. 2007.

[12] F. Agostini, U. Vemulapati, D. Torresin, M. Arnold, M. Rahimo, A. Antoniazzi, L. Raciti, D. Pessina, and H. Suryanarayana, "1MW bi-directional DC solid state circuit breaker based on air cooled reverse blocking-IGCT," in *Proceedings of 2015 IEEE Electric Ship Technologies Symposium (ESTS)*, 2015, pp. 287–292.

[13] R. Zeng, B. Zhao, Z. Q. Yu, Q. Song, Y. L. Huang, Z. Y. Chen, J. P. Liu, W. P. Zhou, and G. Lü, "Development and prospect of IGCT power device in DC grid," *Proceedings of the CSEE*, vol. 38, no. 15, pp. 4307–4317, Aug. 2018.

[14] J. Y. Dai, D. W. Xu, and B. Wu, "A novel control scheme for current-source-converter-based PMSG wind energy conversion systems," *IEEE Transactions on Power Electronics*, vol. 24, no. 4, pp. 963–972, Apr. 2009.

[15] M. Popat, B. Wu, and N. R. Zargari, "A novel decoupled interconnecting method for current-source converter-based offshore wind farms," *IEEE Transactions on Power Electronics*, vol. 27, no. 10, pp. 4224–4233, Oct. 2012.

[16] Y. L. Xue, Z. Xu, W. L. Pan, and F. Wang, "Modeling and simulation for a hybrid current source converter high voltage direct current transmission system," *Automation of Electric Power Systems*, vol. 36, no. 9, pp. 98–103, May 2012.

[17] B. Wu, *High-Power Converters and AC Drives*, Hoboken: Wiley, 2006.

[18] K. D. Luan, Y. H. Li, Z. X. Li, B. Xia, C. Zhao, F. Xu, F. Q. Gao, and P. Wang, "Analysis and design of PWM-CSC for HVDC transmission systems," in *Proceedings of the IECON 2019 - 45th Annual Conference of the IEEE Industrial Electronics Society*, Lisbon, Portugal, 2019, pp. 4773–4777.

[19] B. Xia, Y. H. Li, Z. X. Li, G. Konstantinou, F. Q. Gao, and P. Wang, "Dual phase shift PWM-CSCs based hybrid HVDC transmission system," in *Proceedings of the 2018 IEEE 27th International Symposium on Industrial Electronics (ISIE)*, Cairns, Australia, 2018, pp. 378–383.

[20] B. Xia, Y. H. Li, Z. X. Li, F. Xu, F. Q. Gao, C. Zhao, and P. Wang, "Control strategy of dual current source inverters for high power application under unbalanced grid," in *Proceedings of the 2018 21st International Conference on Electrical Machines and Systems (ICEMS)*, 2018, pp. 1110–1115.

[21] B. Xia, Y. H. Li, Z. X. Li, F. Xu, F. Q. Gao, and P. Wang, "DC fault ride through strategy of a PWM-CSC based hybrid HVDC transmission system," in *Proceedings of 2018 IEEE International Power Electronics and Application Conference and Exposition (PEAC)*, 2018, pp. 1–6.

[22] C. Y. Zhao, J. H. Xia, C. Y. Guo, and R. Q. Zhan, "An improved control strategy for current source converter-based HVDC using fundamental frequency modulation," *International Journal of Electrical Power & Energy Systems*, vol. 133, pp. 107265, Dec. 2021.

[23] K. D. Luan, Y. H. Li, Z. X. Li, J. H. Luo, F. Xu, and P. Wang, "Research on unit power factor operation control strategy of actively commutation converter with switching frequency of 50Hz," in *Proceedings of the 2020 4th International Conference on HVDC (HVDC)*, 2020, pp. 175–178.

[24] X. Wang and B. T. Ooi, "Unity PF current-source rectifier based on dynamic trilogic PWM," *IEEE Transactions on Power Electronics*, vol. 8, no. 3, pp. 288–294, Jul. 1993.

[25] K. D. Luan, Y. H. Li, Z. X. Li, B. Xia, C. Zhao, and P. Wang, "Research on selective harmonic elimination pulse width modulation strategy of actively commutated converter for HVDC applications," *Proceedings of the CSEE*, vol. 40, no. 12, pp. 3970–3979, Jun. 2020.

[26] H. R. Karshenas, H. A. Kojori, and S. B. Dewan, "Generalized techniques of selective harmonic elimination and current control in current source inverters/converters," *IEEE Transactions on Power Electronics*, vol. 10, no. 5, pp. 566–573, Sep. 1995.

[27] C. T. Rim, D. Y. Hu, and G. H. Cho, "Transformers as equivalent circuits for switches: general proofs and D-Q transformation-based analyses," *IEEE Transactions on Industry Applications*, vol. 26, no. 4, pp. 777–785, Jul./Aug. 1990.

Wenwen Zhang received his B.S. degree in 2019 from China Three Gorges University. In 2021, he received his M.S. degree in Electrical Engineering from North China Electric Power University. Now, he is pursuing the Ph.D. degree in North China Electric Power University. His major fields of interest are construction of current source converter HVDC system and equivalent tests of RB-IGCT valve.

Longlong Chen received the B.Sc. and M.Sc. degrees in Xi'an Jiaotong University and Huazhong University of Science and Technology in 2007 and 2009, respectively. Now, he is pursuing the Ph.D. degree in North China Electric Power University. His research interests are DC circuit breakers and transmission line protection.

Xiaoguang Wei received the B.E. and M.E. degrees in Electrical Engineering from North China Electric Power University in 1999 and 2003, respectively, and the Ph.D. degree in Electrical Engineering from China Electric Power Research Institute (CEPRI) in 2010. He joined CEPRI in 2010, where he conducted research on line-commutated converter based high voltage DC (LCC-HVDC) transmission systems and DC breaker used in DC grid. His current research focuses on high-voltage silicon carbide (SiC) power electronic devices based on third-generation power semiconductor materials and the development of new converter equipment.

Lei Qi received the B.S., M.S., and Ph.D. degrees in Electrical Engineering from North China Electric Power University, Baoding, China, in 2000, 2003, and 2006, respectively. He is currently a Professor of Electrical Engineering at North China Electric Power University. His research interests include electromagnetic fields theory and application, electromagnetic compatibility in power systems, and advanced power transmission technology.

Ke Ji received the B.S. degree in Electrical Engineering from Chongqing University, Chongqing, in 2015 and the Ph.D. degree in Electrical Engineering from China Electric Power Research Institute, Beijing, in 2021. From 2021 to 2022, he worked for New York State Center for Future Energy Systems, Rensselaer Polytechnic Institute, Troy, New York and mainly focused on the system design and analysis of renewable energy system. At the end of 2022, he joined North China Electric Power University, Beijing. His current research interests include control design of MMC-HVDC system, and networking stability of the converter-based grid.

Chong Gao received his B.S. degree in 2005 from Yan Shan University. In 2008, he received his M.S. degree from China Electric Power Research Institute (CEPRI). From 2008 to 2012, he is responsible for the research and development of synthetic test circuit for UHVDC thyristor valve and relevant electrical design. Since 2012, he has been working on the development of DC breaker used in DC grid and test method for high power electronic valve based on IGBT. His major fields of interest are research and development of HVDC valve and its test methods.

Zhiyuan He received the B.Eng. degree in Electrical Engineering from Sichuan University, China, in 2000, and the M.Eng. degree and the Ph.D. degree in Electrical Engineering from China Electric Power Research Institute (CEPRI) in 2003 and 2006, respectively. In 2006, he joined CEPRI, where he led the voltage sourced converter based high voltage DC (VSC-HVDC) transmission system group. In the past ten years, he has accomplished theoretical study in high power electronics technology for reliable operation of large interconnected power grids, relocatable DC de-ice systems, DC circuit breakers, and VSC-HVDC transmission, including the first VSC-HVDC project commissioning in 2011 in China and 320 kV/1000 MW voltage sourced converter. He was a member of CIGRE B4 Working Group 48, and conducted research on components testing of VSC system for HVDC applications from 2006 to 2009. He has worked as a member of IEC SC22F WG19, MT22, and WG24 since 2009.